

Characterization of a Superconducting nanowire single photon detector

Max Reicherd

Bachelorarbeit in Physik
angefertigt im Institut für Angewandte Physik

vorgelegt der
Mathematisch-Naturwissenschaftlichen Fakultät
der
Rheinischen Friedrich-Wilhelms-Universität
Bonn

Juli 2024

I hereby declare that this thesis was formulated by myself and that no sources or tools other than those cited were used.

Bonn,
Date
Signature

1. Reviewer: Prof. Dr. Sebastian Hofferberth
2. Reviewer: Prof. Dr. Daqing Wang

Acknowledgements

I would like to thank ...

You should probably use \chapter* for acknowledgements at the beginning of a thesis and \chapter for the end.

Contents

1	Introduction	1
2	Working principle of SNSPDs	2
3	Faint laser source for detector characterization	5
3.1	Characteristics of faint laser sources	5
3.2	Experimental setup	6
4	Characterization of a SNSPD by Single Quantum	9
4.1	Dark Count Rate	9
4.2	Recovery time	11
4.3	Efficiency	15
4.4	Discussion	18
5	Conclusion and Outlook	19
A	Appendix	20
A.1	ND filter calibration	20
A.2	Angle dependent countrate and η_{sde}	21
A.3	Recovery time measurements	22
A.3.1	Recovery time measurements - Oscillating bias current	22
A.3.2	Polarization alignment for system detection efficiency measurements	22
	Bibliography	23

CHAPTER 1

Introduction

CHAPTER 2

Working principle of SNSPDs

This chapter will introduce the working principle of superconducting nanowire single photon detectors (SNSPDs). It provides the principles in terms of their phenomenological aspects. For further details regarding the physics and mathematics behind superconducting nanowires, the reader is directed to the work of Gol'tsman et al [1] and Hadfield et al [2].

The SNSPD has four parts, as shown in figure 2.1. The central detection area is made of a superconducting nanowire ($\approx 100\text{nm}$ wide) on a sapphire base. To collect the whole output of the optical fibre, a pattern out of a thin superconducting film (like niobium nitride) is shaped into a meandering nanowire through nanofabrication [3]. The sapphire layer is used to dissipate the heat when the wire heats up. Further, a gold contact supplies a bias current through the superconducting nanowire and an optical fibre is coupled to the detection area.

To operate the system, the setup is cooled below the critical temperature of the superconductor to 2-3K and a DC current is applied to the nanowire.

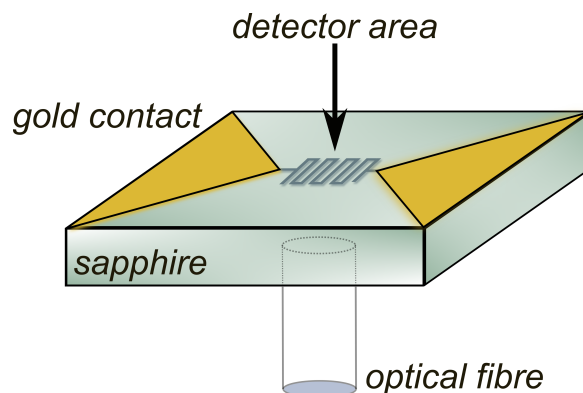


Figure 2.1: (a) Schematic structure of a superconducting nanowire single photon detector [4]

The detection process is shown in the figure 2.2.

Photons hit the superconducting nanowire (ii) and break up individual Cooper pairs. This leads to a local reduction of the critical current below the bias current and in turn to a localised area where the superconductivity is interrupted, this local area forms the so-called "hotspot" (iii). This hotspot forms a resistance area because the critical temperature is exceeded by the energy of the photon. In response,

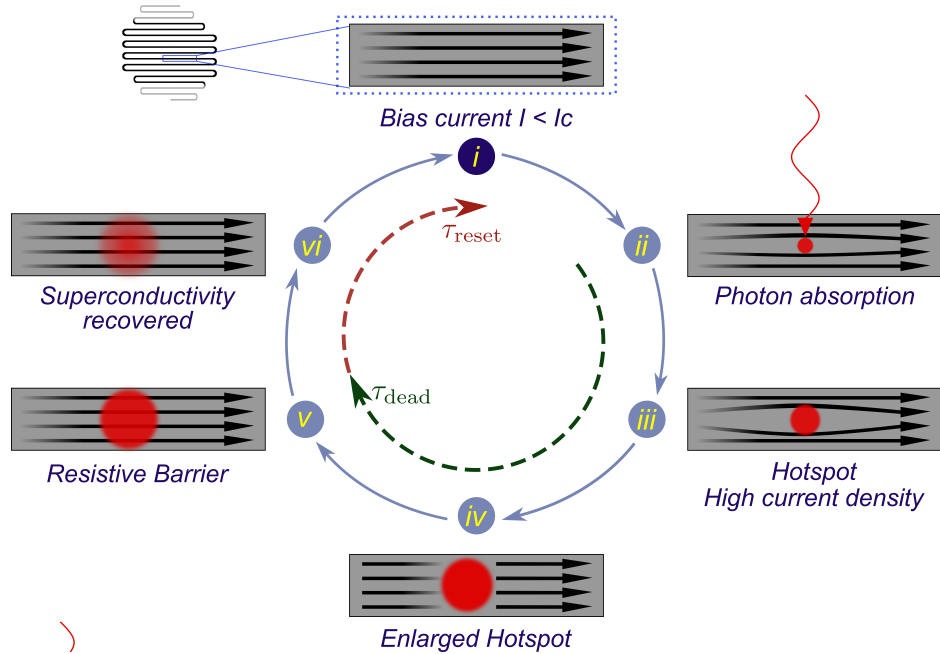


Figure 2.2: Schematic detection cycle of a superconducting nanowire single photon detector [5]

the current flows around this hotspot (iv), whereby the local current density in the side areas next to the hotspot again exceeds the critical current, due to a higher current density. If the critical current is exceeded, the superconductivity also breaks down in these areas. This excess also causes a resistance in the side channels of the nanowire (v). Ultimately, this rapid increase in resistance can be measured in form of a voltage pulse, which can be seen in figure ???. The local non-superconducting area is then cooled down by the cryogenic environment and returns to the superconducting state (iv—i).

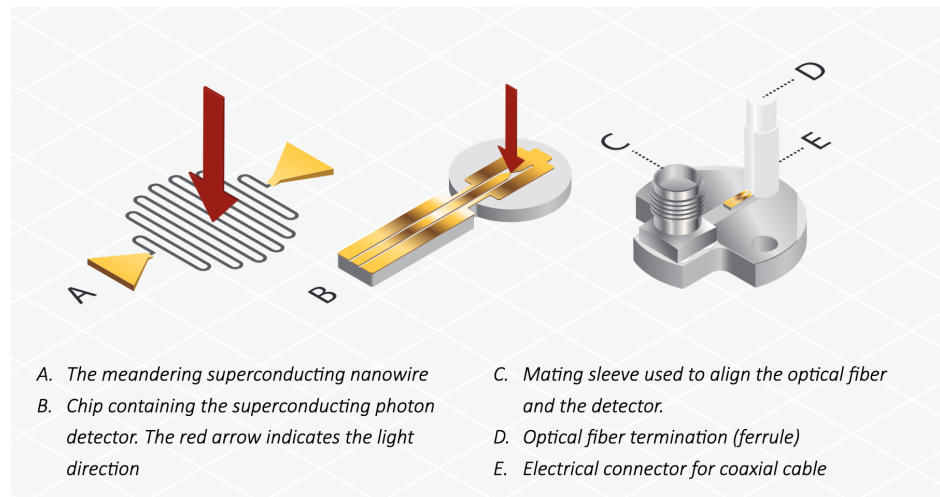


Figure 2.3: Scematic set up of the fiber coupling of a superconducting nanowire single photon detector [Zitieren!](#)

Due to a polarization dependent absorption efficiency it is important to consider the technical detail of the geometry of the meander. In the used SNSPD, the meander design allows for a higher absorption efficiency if the e-field of the photons is parallel polarized to the wire direction than orthogonally polarized ones [3]. As depicted in figure 2.3 the coupled fibre slow axis in the characterized detector is parallel aligned to the nanowire to maximize the absorption efficiency. Other geometries are investigated and might enable a high absorption efficiency independent of the polarization [6].

CHAPTER 3

Faint laser source for detector characterization

In order to characterize a detector, it is necessary to consider not only the characteristics of the detector itself, but also those of the emitter source. This section will focus on the characteristics of the laser setup, which serves as a light source for the detector characterization. In order to provide a brief overview of the characteristics of a coherent laser light source and the conditions it gives for detector characterization, I will first present a summary of the relevant information. Furthermore, I will introduce the setup that I have constructed for characterizing the SNSPD.

3.1 Characteristics of faint laser sources

Using a laser source enables us considering the emitting light as monochromatic beam with angular frequency ω and constant Intensity I . The Photon flux of a laser is defined as the photon average number passing through a cross-section in one unit time:

$$\Phi = \frac{IA}{\hbar\omega} = \frac{P}{\hbar\omega} \text{photons } s^{-1} \quad (3.1)$$

where I is the current of photon, A the cross-section, P the laser power and $\omega = \frac{2\pi c}{\lambda}$ the angular frequency which depends on the wavelength. The average number of registered counts $N(T)$ for a given detection time T by a detector is given by:

$$N(T) = T\Phi\eta = \frac{P T \eta}{\hbar\omega} \text{photons} \quad (3.2)$$

and hence the registered counts \mathcal{R} per unit time is described by:

$$\mathcal{R} = \frac{N(T)}{T} = \eta\Phi = \frac{P\eta}{\hbar\omega} \text{photons } s^{-1} \quad (3.3)$$

where η is the efficiency of the detector system which is described in more detail in section 4.3.

The detector has a maximal detection count rate, and it is restricted by the recovery time ($\tau_{\text{recovery}} = \tau_{\text{rec}}$)[4.2](#) of the detector $\mathcal{R}_{\max} \propto \frac{1}{\tau_{\text{rec}}}$.

Sending too many photons at once to the detector causes latching and prevents counting [3]. Therefore, the photon rate send to the detector has to be below the maximal detection count rate of the detector. As consequence for this experiment, the laser power has to be attenuated to a level where the photon rate is below the maximal detection count rate of the detector.

The photon statistic of coherent light, in our case (in reasonable approximation) of our laser light, is given by poisson statistics.

This property originates from the discrete nature of photons, which are randomly distributed with non-equidistant spacing between each other.

Considering the fact, that the detector is not able to detect photons within the deadtime and with significant lower efficiency in the reset time, one has to look at the probability of photons in those blind spots to include this in later efficiency evaluation.

The amount of photons is calculated by looking at the probability measuring one photon per length segment, given by the deadtime and the reset time. First, we consider one Length segment given by the deadtime τ_d :

$$L_d = c \cdot \tau_d \quad (3.4)$$

$$(3.5)$$

With this, we can calculate for a given measurement time the average photon rate \bar{n} per length segment L_d

$$\bar{n} = \Phi \frac{L_d}{c} = \Phi \cdot \tau_d \quad (3.6)$$

$$(3.7)$$

This enables us to calculate the probability, given by the poisson distribution,

$$P_{\text{dead}}(n) = \frac{(\bar{n})^n}{n!} e^{-\bar{n}} \quad (3.8)$$

of finding n Photons within the length segment, defined by the deadtime τ_d .

In accordance with the specified probability, the quantity of photons that are inherently unmeasurable due to the constraints of the detector can be calculated.

3.2 Experimental setup

From factory details it is known that the recovery time of the detector is located between 17 and 23ns, depending on the detector settings. This details can be confirmed by our measurements as well [4.2](#). This gives a theoretical maximum detection rate with constant maximal possible efficiency of $\mathcal{R}_{\max} \propto \frac{1}{\tau_d} \approx 43 - 58\text{MHz}$. However, this rate would only hold, if the emitter would be a true single photon source with a consistent emitting rate, where photons are equidistantly spaced. Since we use a

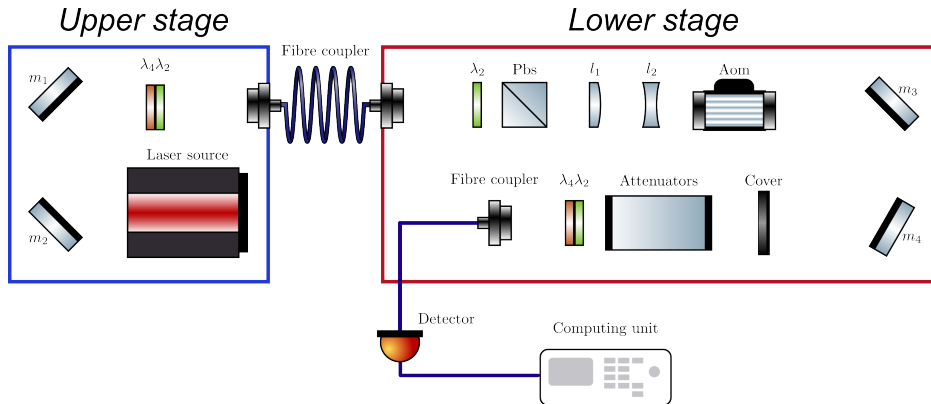


Figure 3.1: Set up for attenuation of a 780nm laser source from the Russian company [Vitawave](#)

coherent laser source the counting rate is significantly lower than the theoretical maximum detection rate. From the factory we got specification of about 2-4 MHz as detection count rate with maximal detection efficiency [Source](#).

The initial situation is that the minimum laser power of the laser source is higher than the maximal detection count rate of the detector. The reason for this is that the laser source does only lase with a constant power with a certain minimum power. Therefore, the laser power can not be regulated down by adjusting the input power of the laser, but has to be attenuated by neutral density filters afterwards.

In order to realize the laser attenuation the setup shown in fig 3.1 was build. The first coupling of the laser light at the upper stage was done in order to operate with the beam on the lower stage, because the laserbeam was due to its construction on an uplifted stage. Afterwards, on the lower stage the beam passes a half-wave plate λ_2 and polarization beam splitter (pbs) to filter the horizontal polarized E-field out. Further, a galilei telescope was build (l_1 and l_2) out of one focal and one diffusing lens for reducing the beam width, so it fits fully on the surface of the crystal of the Acousto-optic modulator (AOM). The first order of the AOM was used for flexible voltage modulation of the laser. A cover was used to filter out the first from the zeroth order of the AOM. Then a flip mount was placed, where Neutral density (ND) filters could be placed in and flexible placed in and out of the laser beam. The ND filters have the function to attenuate the laser light. At the end, before the laser light was again coupled in, again a half-wave plate λ_2 and quarter-wave plate λ_4 were used to stabilize and control the light polarization coupling in the fibre. As mentioned in 2 the light was polarized according to the slow axis of the fibre. Afterwards the light was coupled back into a fibre, so it was directed to the detector. Technically, it was important coupling to a APC/PC to FC/PC optical fibre because the detector only had an FC/PC optical fibre input port, in order to maintain higher efficiency coupling in the light [3].

Besides, this optical setup had to be protected from environmental light. For this, the room where the setup was running was shielded with alu foil which has a reflection coefficient of almost 90% at the operating wavelength of 780nm [Source](#). Moreover, a black box was build. It has the function to avoid further environmental light coupling into the fibre. Additionally, the optical fibre running from the optical setup to the detector was shielded with alu foil as well to avoid absorption from the optical fibre.

Based on those theoretical considerations and our experimental setup, one can approach the central goal to determine the amount of photons and with this, determine the efficiency of the detector.

Central, in order to do efficiency measurements, on the one hand one must send only a few photons (low power) and one must exactly know how many photons are sent. For this we need to measure the power of the laser light, we are sending to the detector. However, the desired light is so weak, we cannot measure it with power-meters or any other measurement devices available to us. So our photon rate we are expecting to send to the detector depends on the ND filters and their optical density (OD) value, since it is the sole factor we can adjust our laser power (here transmission)($T = 10^{-OD}$), hence our amount of photons we send to the detector.

The challenge relying on ND filters is that the fabric values of their OD are not precise, hence the filters need to be calibrated by oneself and as precise as possible, to get accurate and stable OD values for the ND filters.

To get accurate results, the OD value of each filter is measured with two methods to reduce systematic errors. The first method measures the OD values, where the ND filters are set in the flip mount as shown in graph 3.1. The second method measures the OD values after the fibre coupling directly in front of the powermeter outside the blackbox to avoid straying light from the elements in the setup.

The attenuation of ND filters is quantized via the OD value and is connected to the transmission value $T = 10^{(OD)}$ of the outgoing light. Due to the logarithmic definition of the OD value, the OD values of the ND filters are added up when they are stacked on each other.

The measurement of the OD values was done by sending light on the filter and measuring the power with and without the filter. Moreover, only single ND filter measurements were in the measurable range, since the powermeter was not able to measure the power of the attenuated laser light by several stacked ND filters.

The OD value is then calculated by the logarithmic value of the inverse transmission value $\log_{10}(\frac{1}{T})$. The transmission value is given by the proportion of the power with the filter compared without the filter $T = \frac{P_{out}}{P_{in}}$. Afterwards, the final OD values of each method were combined and the corresponding systematic and statistical errors are considered in order to get accurate OD values for the ND filters. Results of the measurements and error calculations can be found in section A.1.

Based on these OD values the photon rate was determined.

CHAPTER 4

Characterization of a SNSPD by Single Quantum

In literature, four central characteristics have emerged to quantify the quality of single photon detectors and make their performance comparable [2, 7]. These characteristics are the system detection efficiency η_{sde} , the dark count rate (DCR), the recovery time ($\tau_{\text{recovery}} = \tau_{\text{rec}}$) and the timing jitter. In this thesis, I focus on the detector efficiency η_{sde} , the dark count rate (DCR) and the recovery time (τ_{rec}). In general there are more than these introduced figures of merits, like after-pulsing but these will not be considered in this thesis.

4.1 Dark Count Rate

The DCR is the rate of measured detection events not intentionally sent from the source (here the faint laser source). It is measured in counts per second and can be caused by statistical fluctuations in the measurement electronics. A low DCR is important for a high signal-to-noise ratio and means easy interpretable results which are not distorted by noise [8].

In the context of SNSPDs, the DCR is dependent on the bias current applied to the nanowire. This is due to the fact that if the bias current approaches the critical current, less current $\Delta I = I_c - I_B$ is needed to exceed the critical current. Therefore, electronic fluctuation, close to the critical current will cause a breakdown of the superconducting state and hence a dark count more often. Furthermore, it is important to perform DCR measurements first in the characterization process because it determines the limit, where general measurements are not distorted by high DCR noise.

Measurement and results

In order to evaluate the DCR, it is necessary to perform measurements in two different setups. First, a setup in which no optical fibre is connected to the detector and the port is covered. In such a setup, it can be assumed that no photons from the surrounding environment are striking the detector. This allows for the measurement of the DCR only triggered by the electronics noise depending on the detector's bias current and trigger voltage.

The required measurement setup consists out of the detector with the protection cap on the output port of the detector. This configuration represents the most shielded environment from external light sources and serves as the reference value for optimal DCR values achievable in single photon

measurements. The measurement was conducted by sweeping the bias current from 0 to $35\mu\text{A}$ in $0.1\mu\text{A}$ increments with an integration time of 200ms at each step

The second setup involves connecting the detector to the faint laser source of section 3.1. The laser source was turned off, so no photons from the source were sent to the detector. This is done in order determine the DCR for consecutive measurements and improve the light shielding of the setup and the optical fibre. This allows one to find the optimal shielding configuration for the highest signal-to-noise ratio. Once more, the bias current was swept from 0 to $35\mu\text{A}$ in $0.1\mu\text{A}$ increments with an integration time of the count rates for 200 ms. In fig ?? the results are shown for an optimized and a non optimized case.

At the initial, non optimized configuration an optical fibre was connected to the detector's output port and the fibre output coupling of the experiment. The laser source was turned off, so only electronic fluctuations and ambient light hitting the detector can cause detection events. To reduce dark counts due to ambient light a black box was constructed that covers the laser setup. Further, the fiber was wrapped in aluminum foil to prevent ambient light to couple to the core through the cladding.

As expected, the DCR rise in each case in ?? with decreasing difference $\Delta I = I_c - I_B$ due to raising probability that weak electronic noises trigger a signal. The orange curve in ?? demonstrates that in the absence of protection, a significant number of photons from the environment are able to enter the detector through various potential pathways like the fibre cladding or the coupling connection to the laser setup.

In contrast, the measurement results with full shielding, depicted in figure 4.1 as well, show, that the DCR of the coupled and protected setup is the same as to the DCR with a cap on. The peaks in the green curve at ≈ 3 and $\approx 14\mu\text{A}$ are artifacts resulting from some leakages in the protection. Nevertheless, these leakages are not substantial when viewed in the context of the total photon count rate, particularly when considering the anticipated photon rates from the faint weak laser source operating in the high kHz and MHz frequency ranges.

Lastly, one can conclude from the investigation of the DCR of channel 1, that all further measurements have to be done at a bias current of $I_B \approx 31.2\mu\text{A}$. As mentioned above the final figure of merit for the DCR is depending on the bias current working point. In this work, five 60s measurements were done for three different bias currents ($24, 28$ and $31.2\mu\text{A}$).

The averaged results for channel one of the detector yield a DCR of:

$$DCR_{24\mu\text{A}} = (5 \pm 0.0001)\text{Hz} \quad (4.1)$$

$$DCR_{28\mu\text{A}} = (4 \pm 0.0001)\text{Hz} \quad (4.2)$$

$$DCR_{31.2\mu\text{A}} = (3 \pm 0.0001)\text{Hz} \quad (4.3)$$

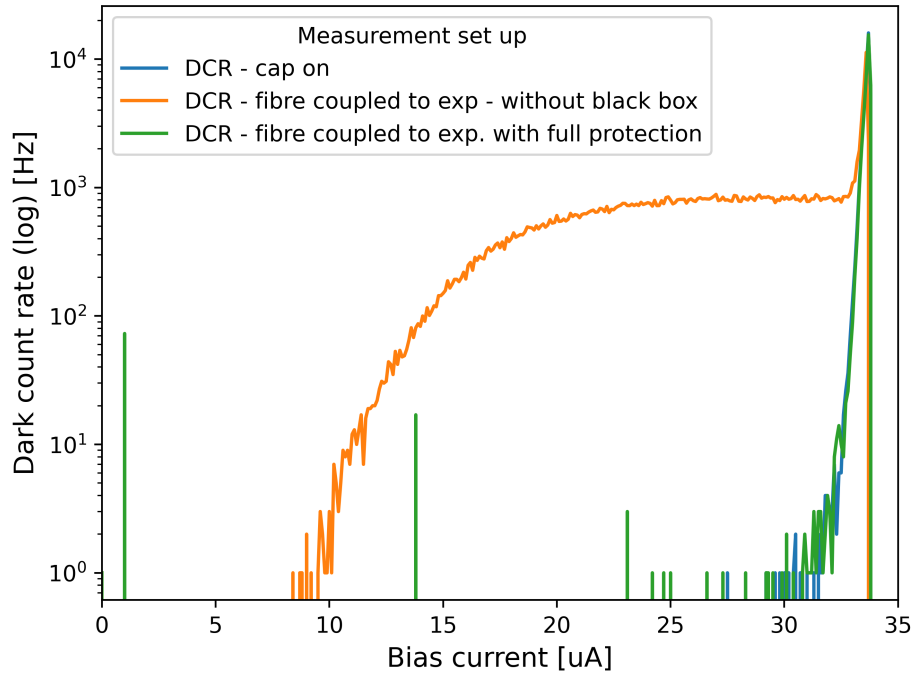


Figure 4.1: Channel 1 DCR measurements for different bias currents at a trigger voltage of 200MHz. The blue curve shows the DCR with a cap on the output port of the detector. The orange curve shows the DCR with a fibre connected to the detector and the fibre output coupling of the experiment. The green curve shows the DCR with a fibre connected to the detector, the fibre output coupling of the experiment and alumini foil wrapped around the optical fibre.

4.2 Recovery time

The concept of the recovery time is visually depicted in fig 4.2. When a photon hits the detector and is absorbed, the efficiency of the detector drops to zero and no further photons can be measured for a certain period of time. This elapsed time is called the dead time $\tau_{\text{dead}} = \tau_d$. The efficiency then rises again to the original device efficiency η_G . This period is called the reset time $\tau_{\text{reset}} = \tau_r$. The vertical dashed line forms the starting point where the efficiency rises again to the original device efficiency η_G . Finally, the sum $\tau_{\text{rec}} = \tau_r + \tau_d$ of both times forms the recovery time τ_{rec} .

The recovery time is important because it determines the rate the detector can detect photons. The lower the recovery time, as higher the counting rate.

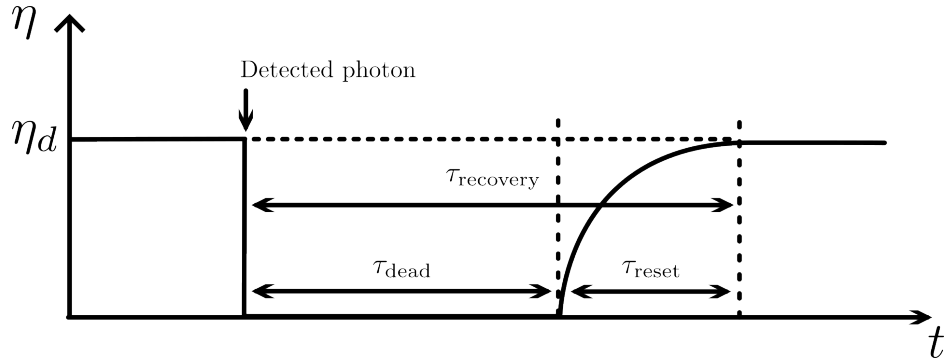


Figure 4.2: Schematic efficiency curve for the detection of a photon[9]. On the Y axis is the efficiency η , where η_{dde} is the device efficiency. On the X axis is the time course of the efficiency. The trajectory of the initial device efficiency, represented by the variable η , does not align with the illustration

Measurement and results

In this work, the recovery time of the detector is determined through an autocorrelation method based on a continuous wave laser source (a faint laser source), a technique that has been previously employed by other research groups. [10, 11]. The measurement was conducted with the setup shown in fig 4.3. The raw analog signals from the detector were directly transmitted to a time tagger unit (Time Tagger 20) by Swabian instruments. with self-adjustable trigger voltages, a device deadtime of 6ns and a maximal counting rate of 9MHz.

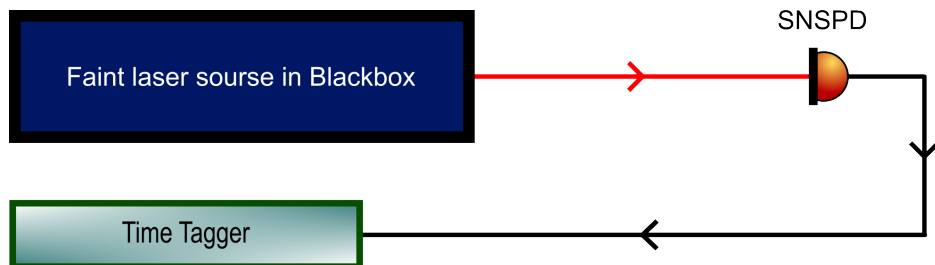


Figure 4.3: Experimental setup for measuring the recovery time. Optical setup of "faint laser source in black box" is depicted in 3.1

This unit enabled the tagging of incoming signals with a time tag, as implied by its name. Subsequently, the tags were used to process the time distances between all signals. The histogram of these distances provide an autocorrelation in time (here not normalized). The autocorrelation was measured for one channel for four different bias currents ($25\mu\text{A}$, $27\mu\text{A}$, $29\mu\text{A}$ and $31.2\mu\text{A}$) and trigger voltages from 300mV to 900mV in 100mV steps.

These measurements were done to determine the recovery time and analyze its dependencies. The results for a fixed bias current of $31.2\mu\text{A}$ are shown in figure 4.4(a) and for $26\mu\text{A}$ in 4.4(b). The other measurement results are presented in the appendix A.3.

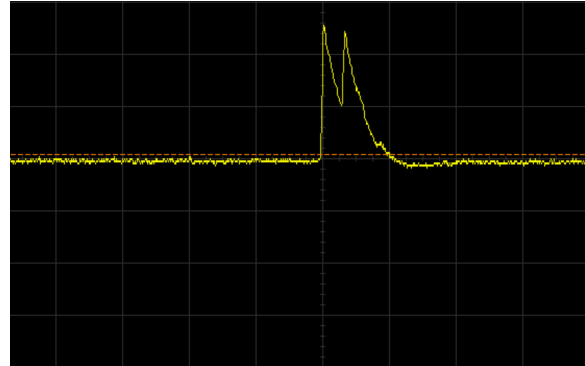


Figure 4.5: Analog signal screenshot of an oscilloscope from channel 1 for a bias current of $31.2\mu\text{A}$ and a trigger of 600mV . X-axis: time in 50ns steps (straight vertical yellow lines), Y-axis voltage in 500mV steps (straight horizontal yellow lines)

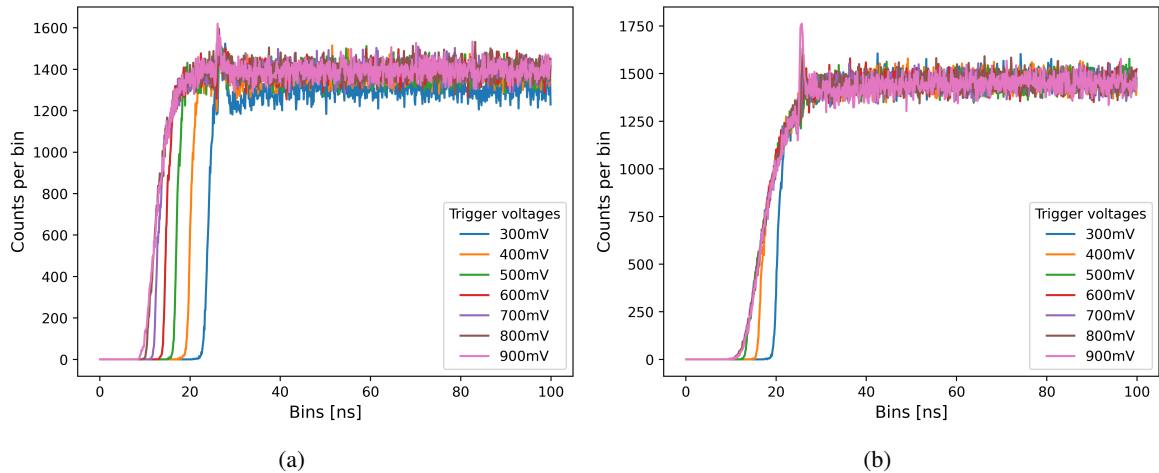


Figure 4.4: Autocorrelation of distances between two photon detection events for (a) $I_B = 31.2\mu\text{A}$ and (b) $I_B = 25\mu\text{A}$. The X-axis represents the time distance between two signals in 1ns steps and the Y-axis the counts per bin.

The results of the autocorrelation show three major features. First, for low trigger voltages, the dead time is longer and decrease for increasing trigger voltages. This is true for both, the lower and higher bias current. The reason for this behavior can be explained best by looking at an exemplary raw analog signal (see fig 4.5) of two consequent pulses. In figure 4.5 one can see the peaks of two consecutive detection signals, where the second pulse starts ($\approx 20\text{ns}$) before the falling edge of the first pulse ends. Physically, that means, that before the first signal spike has fully decayed a second photon, already hit the detector, got detected and produced a second spike.

If the trigger is below 500mV the time tagger will count this signal as one count, since the second pulse came when the remaining voltage of the wire was above 500mV . If the trigger is above 500mV both pulses will be counted. This allows successive events with smaller time delay between them and therefore reduces the perceived recovery time.

Secondly, for the lower bias current ($26\mu\text{A}$), the rising count curves for each trigger voltage converge

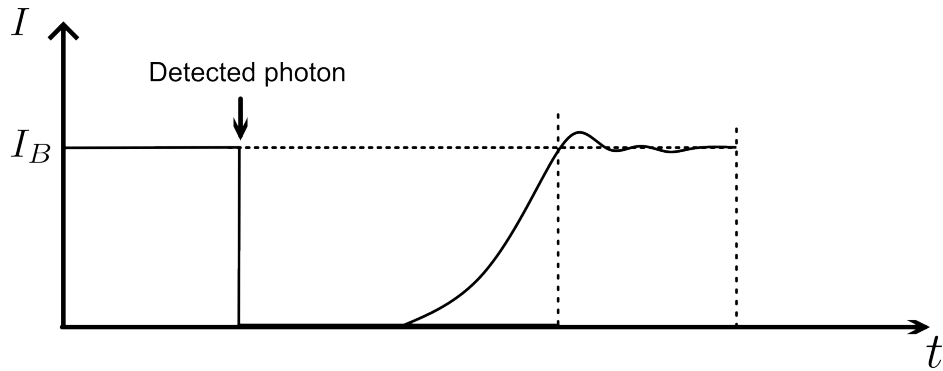


Figure 4.6: A sketch of the assumed bias current behaviour is presented herewith. Once the bias current has been reached, the current undergoes a brief oscillation before stabilising at the bias current level.

earlier in comparison to the bias current of $31.2 \mu\text{A}$. At the bias current of $31.2 \mu\text{A}$, the four different count curves remain distinct until they reach their peak. This can be attributed to the differing pulse heights, dependent on the bias current. According to Ohm's law, for the same resistivity, a lower bias current corresponds to lower voltage pulses and vice versa. Due to the lower pulse, the regime, where pulses can be resolved by a trigger voltage of 600mV but not 500mV becomes smaller. The different pulse heights can also be verified by the recorded analog signals shown in figure: ??.

The third interesting feature is the count peak at $24\text{-}27\text{ns}$ for $31.2\mu\text{A}$ and a trigger level of 300 mV 4.4(a).

This small peak is less visible at lower bias currents or higher trigger levels. Closer examination of this trend are shown in the appendix A.

This behavior can be understood by taking into account that the bias current needs a finite amount of time to reach its target value once the superconductivity is restored and will also overshoot a bit after reaching the target value. A sketch of the expected behavior is shown in figure 4.6.

Following the detection of a current, the course of the current does not proceed directly and precisely to the bias current. Instead, it oscillates for a brief period and then rapidly reaches equilibrium.

If the target bias current is close to the critical current the overshooting might cause a breaking of the superconductivity leading to a time correlated increase in the dark current rate (seen in figure 4.1). This feature is less severe for higher trigger voltages which suggests that the self triggered pulse is typically of smaller height.

It can be concluded that the optimal recovery time is achieved when the detector is operated at a bias current maintained at a level that is close but not excessive to critical current of $31.2\mu\text{A}$ and a trigger voltage of 600v .

This enables the generation of a higher pulse, which in turn results in a steeper reset time, a shorter dead time, and consequently, a shorter recovery time.

DISCLAIMER: ALL THE RESULTS AND METHODS ARE NOT FINALIZED AND WILL BE ADAPTED, IF METHOD IS AGREED

Finally, a reasonable trigger point for a bias current of $31.2\mu\text{A}$ is 600mV , which yields the lowest recovery time. The calculation of the τ_{rec} is done, by calculating the average of counts per bin from $30\mu\text{A}$ till the end of the measurement period. Here, I choose $30\mu\text{A}$ as the starting point, because from this point a constant curve is visible (saturation point). Furthermore, I fitted a function to estimate the point were 50% and 90% of the full efficiency is reached. Moreover, the raise of the function

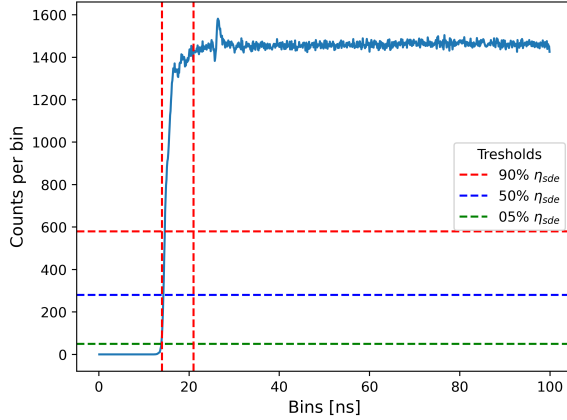


Figure 4.7: Histogram of distances between signals for $I_B = 31.2\mu A$ and 600mV. H- and v-lines indicate the dead-; reset- and recovery time

for the dividing line between dead and reset time is calculated by the point where the gradient of the fitting function is not zero any more. The calculated points are visualized in fig: 4.7 and the final recovery time is $\tau_{rec}^{90\%} = (21.21 \pm 0.34)ns$, where $\tau_d = (14.13 \pm 0.14)ns$ is the dead time and $\tau_r = (7.08 \pm 0.36)ns$ the reset time. Moreover, the time the detector is back at efficiency of $\eta_{sde} = 50\%$ is $\tau_{rec}^{50\%} = (18.21 \pm 0.24)ns$.

4.3 Efficiency

There are three types of efficiencies that describe independent loss processes in single photon detection. Efficiency is a way of measuring how likely a process is to happen. There are three main types of efficiency: the coupling efficiency (η_C), the absorption efficiency (η_A) and the registration efficiency (η_R). The graph 4.8 shows schematically where the different losses in the detection process appears. When a photon is sent to a detector via an optical fibre, not all photons can be coupled into the fibre. The probability of coupling is the so called the *coupling efficiency*. When photons hit the detector, there is always a probability that the photon will not be absorbed by the detector. This is due to material and symmetry properties like the design of the superconducting nanowire [7]. This is described by the *absorption efficiency*. Finally, there is always a probability that the photon will not be registered by the measuring electronics. This is expressed with the *registration efficiency*.

In literature, these terms are summarized in two general efficiency terms: the device detection efficiency ($\eta_{dde} = \eta_A \cdot \eta_R$) and the system efficiency ($\eta_{sde} = \eta_A \cdot \eta_R \cdot \eta_K$) [2, 7]. The device detection efficiency η_{dde} corresponds to the efficiency of the device itself and neglects coupling inefficiencies. This gives an idealized upper bound to the achievable efficiency. For perfect optical coupling, the device detection efficiency is equal to the system detection efficiency ($\eta_{dde} = \eta_{sde}$). The system detection efficiency η_{sde} takes the coupling losses to the optical fibre into account. This is the case if the detector is connected to a fibre, as the device properties or the experiment does not allow photon detection in a free environment.

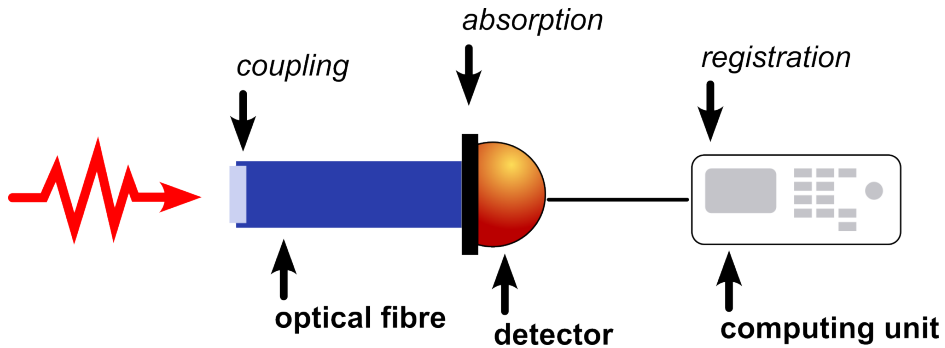


Figure 4.8: Sketch of the components in the detector setup where photonlosses appear and consequently a probability (η_K , η_A or η_R) has to be considered.

Measurement and results

In the given setup, only the system detection efficiency η_{sde} is measured, because the detector is already prebuild with a fixed coupling to a fibre [3]. This internal fibre is connected to a single mode fibre to fibre port for the connection type FC/PC (fibre channel / physical contact). Through this, one can connect the detector with an external optical fibre and send photons from the experiment to the detector.

The system detection efficiency η_{sde} will depend on the applied bias current, the chosen trigger voltage and the photon rate and the photon polarization. Here, all these dependencies will be investigated to characterize the system detection efficiency. Each measurement was done in the setup explained in part 3.

The measurements were done in a specific order, since the conclusions drawn for certain measurements influence the preceding measurements. Based on this, it is first necessary to align the polarization of the laser light with the slow axis of the fibre connected to the output port of the detector. According to the manual the coupled light needs to polarized along the slow axis of the fibre [3]. This is explained by the fact that the absorption efficiency η_A is maximized when the light is polarized parallel to the superconducting nanowire of the detector as explained in 2.

A combination of a quarter-wave plate and a half-wave plate is used to alter the polarization of the input laser light. The quarter-wave plate is used to pre compensate the stress induced birefringence of the fiber input while the half-wave plate is used to rotate the linear input polarization. The measurement of the polarization was done with the polarization analyzer SK010PA by Schäfter + Kirchhoff Schäfter + Kirchhoff. Furthermore, the laser power input was set to $511.1 \mu\text{V}$ and attenuated by three ND filters with a total OD of 9.574, in order to make sure that the detector can reach high count rates as considered in 3.2. Different polarization angles for measuring the countrate of the detector are then realized by rotating the half-wave plate while the quarter wave plate is kept in its position. Final alignment of the polarization are shown in the Appendix A.3.2.

By adjusting the laser beam linear with a quarter-wave plate first and rotating the half-wave plate in $(10 \pm 2)\text{deg}$ steps afterwards, the polarization axis was rotated relative to the slow axis of the fibre. With this, it was possible to find the angle configuration were the maximum of light was coupled to the slow axis of the fibre. This is important since measuring subsequent efficiency measurements aligned to a different axis would put a systematic downshift on the true efficiency of the detector. In the figures 4.9(b) the count rate and the resulting system detection efficiencies are depicted.

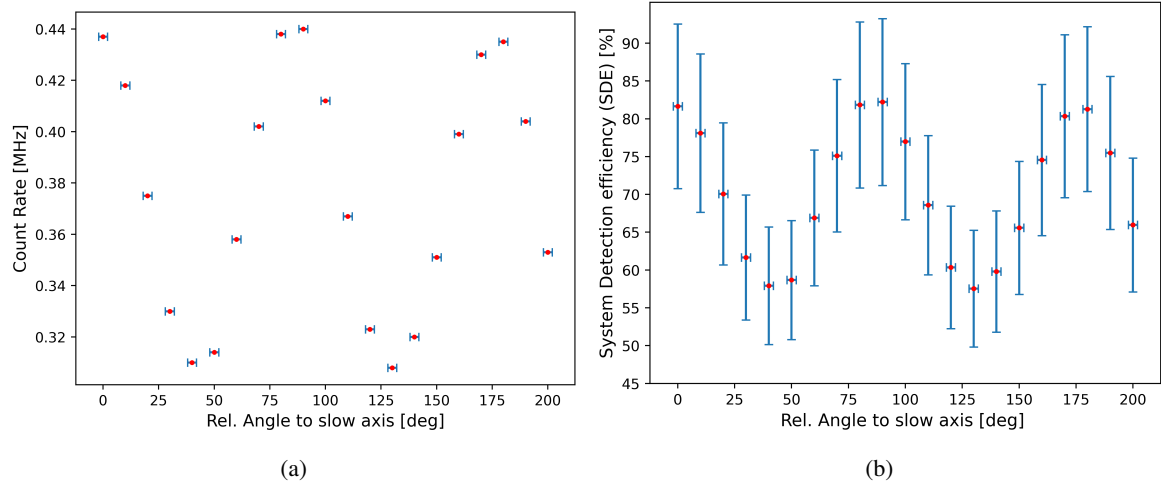


Figure 4.9: On both X axis the relative angle to the slow axis is depicted. (a) shows the angle dependent countrate, (b) shows the angle dependent η_{sde} . Countrate error in (a) and corresponding $\Delta\eta_{\text{sde}}$ in (b) are depicted in table A.1 and A.2 and are calculated according considerations mentioned in A.1

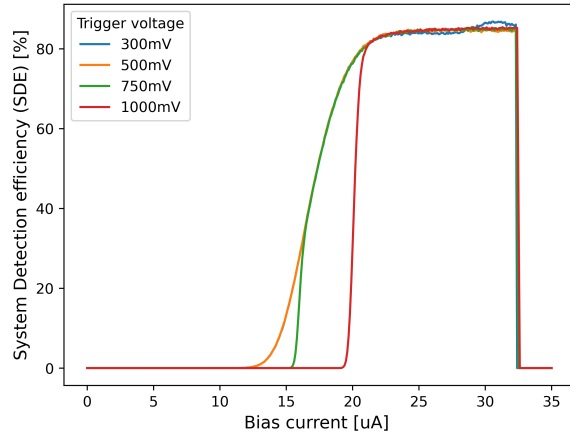


Figure 4.10: System detection efficiency for different bias currents and trigger voltages

For preceding measurements the polarization was aligned to an angle, where a maximum of $\eta_{\text{sde}} = 81.652 \pm 10.872$ was reached.

From now on for the following measurements, the polarization angle which yields the highest efficiency was used.

In a second measurement the trigger voltage and bias current dependency was investigated. For this the bias current was swept from 0 to 35 μA in 0.1 μA steps and events within 200ms integration time were counted.

In fig 4.10 one can see that at lower trigger voltage of 300mV the count rate oscillates a bit, which again corresponds likely to the increased dark count rates as explained in 4.6. Furthermore, one can see that for lower trigger voltages the detected counts for lower bias currents are higher. This is due to the consideration of lower voltage pulses in lower bias current regimes if the trigger voltage

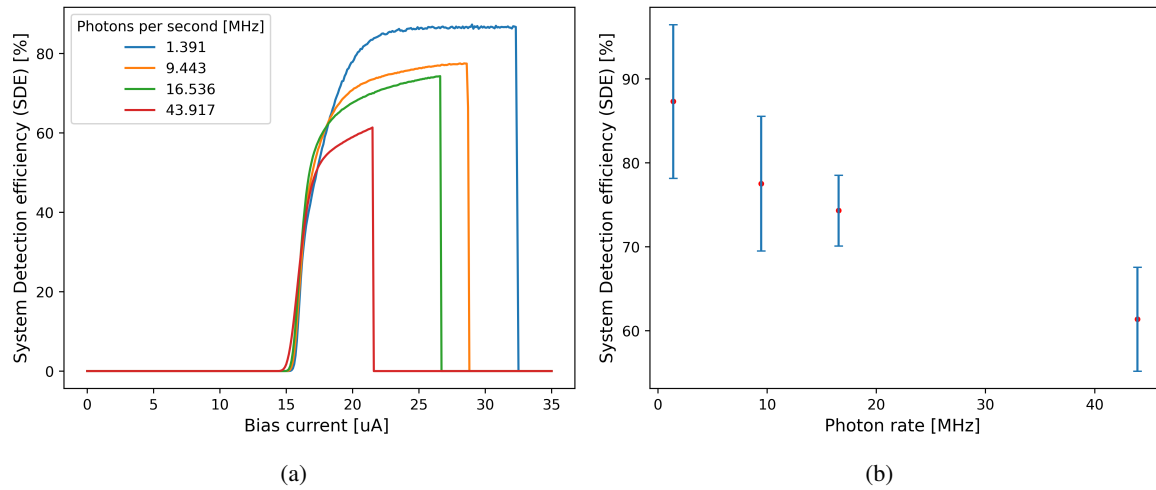


Figure 4.11: (a) Course of system detection efficiency for different bias current and count rates (b) Course of system detection efficiency for different count rates

is low. Hence, with a lower trigger voltage one can count already signals, however, with a very low system detection efficiency η_{sde} . Another behaviour is the saturation, which is reached by each trigger voltage configuration at around $I_{\text{Bias}} \approx 20\mu\text{A}$. Here the maximum count rate is reached and the efficiency course continues constant without any gradient. At the end at a bias current of $I_{\text{Bias}} \approx 32\mu\text{A}$ the efficiency drops. This is because the critical current is reached. After this, according to the [manual_single_quantum_snspd], the detector stops sending countable analog signals, which corresponds to an efficiency of zero.

Finally, measurements for different count rates were done, to determine the bandwidth where the photons are detected with the highest efficiency. The count rates were varied by using different ND filters and was done by putting together different ND filter combinations in order to get different OD values and therefore different count rates. To avoid the oscillation of count rates near the critical current as seen in fig 4.10 a trigger voltage of 750mV is used.

In fig 4.11(a) one can see that the system detection efficiency is decreasing with increasing count rates. Moreover, only for the measurement of 1.391MHz one gets a range of bias currents where the efficiency is constant. All the other measurements with higher count rates show a continues increase in η_{sde} up to the point the detector shut down. Furthermore, the shut-down happens earlier, when the count rate is higher. This dynamics follows from the fact that the detector is not able to recover in time, when the count rate is too high. Hence, the critical temperature is reached earlier, when the count rate is raising and the detections is shut down.

In fig 4.11(b) the maximum system detection efficiency for each count rate is shown. One can see clearly a downward trend for raising count rates. Moreover, the measurement shows the saturating and therefore a maximal system detection efficiency of $(87.308 \pm 9.159)\%$ for channel 1. This η_{sde} is reached at a count rate of $1.391 \pm 0.32\text{MHz}$.

4.4 Discussion

CHAPTER 5

Conclusion and Outlook

APPENDIX A

Appendix

A.1 ND filter calibration

To calculate the OD value of the ND Filters, we first calculate the Transmission value:

$$T = \frac{P_{detected}}{P_{input}}$$

For the Error calculation we have to consider two error sources. Once the measurement uncertainty of the photodiode and the measurement uncertainty from reading the value from the Powermeter. Since the uncertainty from the photodiode is always 3% of the measured value, it does not contribute to the error, since the transmission is a division and this does not affect the overall relation. However, reading of the value from the powermeter provides always a different error because the last displayed order of magnitude of the displayed result on the powermeter fluctuates.

Its also important to mention that after each adjustment for the fiber coupling, it was not possible to get to the same initial value. Therefore, we always have different power values we compare, though the filtering process was done always with the same amount of light power. So we have to consider an error from the fiber coupling and optimization. For this our P_{input} value for the Transmission is in reality not the measured value we coupled in but the averaged value with an standard deviation as error. Also, this only applies for the first measurement method because we adjust there our fiber coupling. In the second measurement we have a stable P_{input}

So for the transmission error we got:

$$\Delta T = \sqrt{\left(\frac{\Delta P_{detected}}{P_{input}}\right)^2 + \left(\frac{\Delta P_{input} P_{detected}}{P_{input}^2}\right)^2} \quad (\text{A.1})$$

Where.

$$\Delta P_{Input} = \sqrt{(P_{detected}^{Pow.meterreadoff})^2 + (P_{detected}^{STD,coupling})^2} \quad (\text{A.2})$$

And with the relation: $OD = \log(\frac{1}{T})$ we can calculate the error for the OD: $\Delta OD = \frac{\Delta T}{\ln(10) \cdot T}$

Appendix A Appendix

Regarding the errors it is important to mention that the error of the photodiode is not relevant if we look at the error of the transmission rate because its the same for the measurement before and after the ND Filters.

In general the measurement error of the photodiode is about 3% of the measured value [Powermeter specs](#). This error I considered only in the calculation for the output power error:

Table with measurement values and results for Transmission value and OD Value

ID	Expectedt OD Value	Measured T Value	T_Value Error Systematic	T Value Error stat	T Value Error	Mean OD Value	OD Value Error
TP03337667	1,00	1,43E-01	67,697E-4	3,223E-03	7,50E-03	0,844	0,023
TP03337667 (2)	1,00	1,47E-01	50,474E-04	3,073E-03	5,91E-03	0,832	0,017
TP03366490	3,00	8,26E-03	32,418E-05	1,882E-04	3,75E-04	2,083	0,020
TP03366490 (2)	3,00	7,93E-03	52,291E-05	1,744E-04	5,51E-04	2,101	0,030
TP03275234	4,00	1,00E-03	5,318E-05	4,381E-05	6,89E-05	2,999	0,030
TP03312353	4,00	1,04E-03	7,142E-05	4,312E-05	8,34E-05	2,983	0,035
TP03271009	4,00	1,02E-03	4,842E-05	4,432E-05	6,56E-05	2,991	0,028
TP03275234 (2)	4,00	1,03E-03	6,566E-05	4,303E-05	7,85E-05	2,986	0,033
TP03324728	5,00	1,80E-04	9,945E-06	3,843E-05	3,96E-05	3,744	0,095
TP03287742	5,00	1,78E-04	4,196E-06	3,731E-05	3,75E-05	3,749	0,092
TP03348187 (2)	5,00	1,82E-04	4,506E-06	3,921E-05	3,95E-05	3,739	0,094
TP03348187	5,00	1,82E-04	5,792E-06	3,862E-05	3,91E-05	3,739	0,093

Calculating the error for stacked ND filters. The Error from

$$P_{input} = P_{Input}^{initial} \cdot 10^{-OD} \quad (A.3)$$

constructed out of the uncertainty of the Photodiode $\Delta P_{Input}^{initial} = 0.03 \cdot P_{Input}^{initial}$ and the error of the ND Filters

$$\Leftrightarrow \Delta P_{input} = \sqrt{(\Delta P_{Input}^{initial} \cdot 10^{-OD})^2 + (P_{Input}^{initial} \cdot \log(10) \cdot \Delta OD)^2} \quad (\text{A.4})$$

The Error $\Delta P_{detected}$ is reformulated to a rate only in the order of a few hundred Herz and is neglectable compared to the ΔP_{input} .

A.2 Angle dependent countrate and η_{sde}

Table A.1: Angle Dependent countrate results

Table A.2: Angle Dependent SDE Results

A.3 Recovery time measurements

A.3.1 Recovery time measurements - Oscillating bias current

A.3.2 Polarization alignment for system detection efficiency measurements

Method 1 and 2 combined: In both tables above one can see that the second method has slightly higher values. This indicates a systematic error we don't know. Till now, we only considered statistical errors. Now if we want to calculate the true value we have to consider the systematic error as well. Here we determine the systematic error as half of the difference between the values from method one and method two $\Delta T_{syst} = \frac{T_{meth_2} - T_{meth_1}}{2}$. So the final transmission error of the combined measurements is: $\Delta T = \sqrt{\Delta T_{stat}^2 + \Delta T_{syst}^2}$

In the appendix you usually include extra information that should be documented in your thesis, but not interrupt the flow.

Bibliography

- [1] G. N. Gol'tsman et al., *Picosecond superconducting single-photon optical detector*, *Applied Physics Letters* **79** (2001) 705, URL: <https://doi.org/10.1063/1.1388868> (cit. on p. 2).
- [2] C. M. Natarajan, M. G. Tanner and R. H. Hadfield, *Superconducting nanowire single-photon detectors: physics and applications*, *Superconductor science and technology/Superconductor science technology* **25** (2012) 063001, URL: <https://doi.org/10.1088/0953-2048/25/6/063001> (cit. on pp. 2, 9, 15).
- [3] Single Quantum, *Single Quantum EOS User Manual*, 2022 (cit. on pp. 2, 3, 6, 7, 16).
- [4] G. A. Steudle et al., *Measuring the quantum nature of light with a single source and a single detector*, *Physical review. A, Atomic, molecular, and optical physics/Physical review, A, Atomic, molecular, and optical physics* **86** (2012), URL: <https://doi.org/10.1103/physreva.86.053814> (cit. on p. 2).
- [5] singlequantum.com, *Superconducting Nanowire Single Photon Detectors Operation principle*, <https://singlequantum.com/wp-content/uploads/2023/06/Single-Quantum-Operation-Principle-print.pdf>, Accessed: 2023-06, n.d. (Cit. on p. 3).
- [6] F. Zheng et al., *Design of a polarization-insensitive superconducting nanowire single photon detector with high detection efficiency*, *Scientific reports* **6** (2016), URL: <https://doi.org/10.1038/srep22710> (cit. on p. 3).
- [7] R. H. Hadfield, *Single-photon detectors for optical quantum information applications*, *Nature photonics* **3** (2009) 696, URL: <https://doi.org/10.1038/nphoton.2009.230> (cit. on pp. 9, 15).
- [8] Wikipedia contributors, *Signal-to-noise ratio*, 2024, URL: https://en.wikipedia.org/wiki/Signal-to-noise_ratio (cit. on p. 9).
- [9] K. Shalm et al., *Single-Photon Detector Tutorial*, Computer Scientist QCRYPT, National Institute of Standards and Technology, 2013, URL: <https://qcrypt.github.io/2013.qcrypt.net/contributions/Shalm-slides.pdf> (cit. on p. 12).
- [10] C. Autebert et al., *Direct measurement of the recovery time of superconducting nanowire single-photon detectors*, *Journal of applied physics* **128** (2020), URL: <https://doi.org/10.1063/5.0007976> (cit. on p. 12).

Bibliography

- [11] S. Miki, M. Yabuno, T. Yamashita and H. Terai, *Stable, high-performance operation of a fiber-coupled superconducting nanowire avalanche photon detector*, *Optics express* **25** (2017) 6796, URL: <https://doi.org/10.1364/oe.25.006796> (cit. on p. 12).